Bioactive Materials 34 (2024) 366–380

Contents lists available at ScienceDirect

Bioactive Materials

journal homepage: www.keaipublishing.com/en/journals/bioactive-materials

Neddylation suppression by a macrophage membrane-coated nanoparticle promotes dual immunomodulatory repair of diabetic wounds

Ruiyin Zeng [a,1], Bin Lv [a,1], Ze Lin [a,1], Xiangyu Chu [a,1], Yuan Xiong [a], Samuel Knoedler [b], Faqi Cao [a], Chuanlu Lin [a], Lang Chen [a], Chenyan Yu [a], Jiewen Liao [a], Wu Zhou [a], Guandong Dai [c,**], Mohammad-Ali Shahbazi [d,e,***], Bobin Mi [a,****], Guohui Liu [a,*]

[a] Department of Orthopedics, Union Hospital, Tongji Medical College, Huazhong University of Science and Technology, Wuhan, 430022, China
[b] Institute of Regenerative Biology and Medicine, Helmholtz Zentrum München, 81377, Munich, Germany
[c] Department of Orthopaedics, Pingshan District People's Hospital of Shenzhen, Pingshan General Hospital of Southern Medical University, Shenzhen, Guangdong, 518118, China
[d] Department of Biomedical Engineering, University Medical Center Groningen, University of Groningen, Antonius Deusinglaan 1, 9713 AV, Groningen, the Netherlands
[e] W.J. Kolff Institute for Biomedical Engineering and Materials Science, University of Groningen, University Medical Center Groningen, Antonius Deusinglaan 1, Groningen, 9713 AV, the Netherlands

ARTICLE INFO

Keywords:
Diabetes
Biomimetic nanoparticle
Macrophage polarization
Macrophages cell membranes
Wound healing

ABSTRACT

Oxidative stress, infection, and vasculopathy caused by hyperglycemia are the main barriers for the rapid repair of foot ulcers in patients with diabetes mellitus (DM). In recent times, the discovery of neddylation, a new type of post-translational modification, has been found to regulate various crucial biological processes including cell metabolism and the cell cycle. Nevertheless, its capacity to control the healing of wounds in diabetic patients remains unknown. This study shows that MLN49224, a compound that inhibits neddylation at low concentrations, enhances the healing of diabetic wounds by inhibiting the polarization of M1 macrophages and reducing the secretion of inflammatory factors. Moreover, it concurrently stimulates the growth, movement, and formation of blood vessel endothelial cells, leading to expedited healing of wounds in individuals with diabetes. The drug is loaded into biomimetic macrophage-membrane-coated PLGA nanoparticles (M-NPs/MLN4924). The membrane of macrophages shields nanoparticles from being eliminated in the reticuloendothelial system and counteracts the proinflammatory cytokines to alleviate inflammation in the surrounding area. The extended discharge of MLN4924 from M-NPs/MLN4924 stimulates the growth of endothelial cells and the formation of tubes, along with the polarization of macrophages towards the anti-inflammatory M2 phenotype. By loading M-NPs/MLN4924 into a hydrogel, the final formulation is able to meaningfully repair a diabetic wound, suggesting that M-NPs/MLN4924 is a promising engineered nanoplatform for tissue engineering.

1. Introduction

Diabetes, a persistent metabolic disorder, presents a significant threat to the overall well-being of individuals, both physically and mentally. Recent studies show that 1 in 10 adults worldwide suffers from diabetes, which is expected to increase to more than 780 million in the next 25 years [1,2]. Due to oxidative stress, infection, vascular disease, and inflammation caused by hyperglycemia-induced metabolic disorders [3], patients with diabetes mellitus (DM) often have poor wound healing and develop diabetic foot ulcers (DFUs), which can lead to amputation in severe cases [4]. Therefore, much effort has been devoted to understanding the pathogenesis of diabetic wounds and novel treatments. Recent research has discovered methods to speed up the healing

Peer review under responsibility of KeAi Communications Co., Ltd.
* Corresponding authors.
** Corresponding author.
*** Corresponding author. Department of Biomedical Engineering, University Medical Center Groningen, University of Groningen, Antonius Deusinglaan 1, 9713 AV, Groningen, the Netherlands.
**** Corresponding author.
E-mail addresses: kerdong1976@hotmail.com (G. Dai), m.a.shahbazi@umcg.nl (M.-A. Shahbazi), mibobin@hust.edu.cn (B. Mi), liuguohui@hust.edu.cn (G. Liu).
[1] These authors contributed equally to this article.

https://doi.org/10.1016/j.bioactmat.2023.12.025
Received 21 October 2023; Received in revised form 19 December 2023; Accepted 28 December 2023

Abbreviations

NPs/MLN4924	PLGA-coated MLN4924 nanoparticles
M-NPs/MLN4924	Macrophage membrane-coated NPs/MLN4924 nanospheres
GelMA@ M-NPs/MLN4924	M-NPs/MLN4924 nanoparticles loaded by porous GelMA hydrogel
CRL	Cullin-RING E3 ligase
EGF	Epidermal growth factor
LPS	Lipopolysaccharide
IL-6	Interleukin-6
IL6-R	Interleukin-6 receptor
TNF-α	Tumor necrosis factor-alpha
TNFR1	Tumor necrosis factor receptor 1
TLR4	Toll-like receptor 4
TEM	Transmission electron microscopy
DLS	Dynamic light scattering
CCK-8	Cell Counting Kit 8
iNOS	Inducible nitric oxide synthase
ARG1	Arginase 1
RT-PCR	Real-time polymerase chain reaction
ELISA	Enzyme-linked immunosorbent assay
NF-κB	Nuclear factor-κB
IκBα	Inhibitor of NF-κB-alpha
NF-κB	Nuclear factor-κB
VEGF-A	Vascular endothelial growth factor A
PBS	Phosphate-buffered saline
DAPI	4',6-Dimidazole-2-phenylindole
FITC	Fluorescein isothiocyanate
APC	Allophycocyanin
PE	Phycoerythrin
H&E	Hematoxylin and eosin
HUVECs	Human umbilical vein endothelial cells

of wounds in diabetic individuals by suppressing long-lasting inflammation and the polarization of M1 macrophages (known for their pro-inflammatory properties), as well as boosting angiogenesis to enhance the delivery of nutrients and oxygen to diabetic wounds [5–7].

Neddylation, a protein modification that occurs after translation, was recently discovered. A reversible post-translational modification similar to ubiquitination, neddylation involves the covalent attachment of the ubiquitin-like protein NEDD8 to specific lysine residues on target proteins. Neddylation and ubiquitination share the commonality of attaching a small protein to lysine residues, yet they diverge in terms of their functions and the proteins they target. The process of neddylation primarily involves the activation of NEDD8 E1 enzyme (NAE), the conjugation of NEDD8-specific E2 enzyme (UBC12), and the transfer of NEDD8 to cullin proteins by NEDD8 E3 ligase in a sequential manner. Neddylation regulates many biological functions, including protein subcellular localization, protein stability, and activity [8]. Furthermore, it represents a promising therapeutic target in the pursuit of remedies for various afflictions (Scheme 1A) [9].

MLN4924 (Pevonedistat) is the first small molecule inhibitor of NAE that has entered clinical trials for various cancer treatments [10]. It blocks NAE-mediated neddylation by forming a NEDD8-MLN4924 adduct, thereby reducing the neddylation of cullins and other protein substrates. Research has indicated that it has the potential to induce harm to DNA, halt the cell cycle, and trigger both cell death and aging in tumor cells [11–13]. Furthermore, studies have demonstrated that nanomolar concentrations of MLN4924 induce the growth, renewal, and specialization of stem cells in both cancerous and non-cancerous stem cell models. Additionally, it enhances the healing of skin wounds and the migration of immortalized epithelial cells in EGF-induced mouse models [14]. Moreover, the partial inhibition of neddylation by MLN4924 at low concentrations inhibited the LPS-induced production of pro-inflammatory cytokines by RAW 264.7 macrophages [15]. However, higher doses of MLN4924 consistently and severely inhibited neddylation and subsequently inhibited macrophage viability [16]. To date, whether neddylation is involved in the dysregulation of diabetic wound repair and whether the inhibition of MLN4924-mediated neddylation contributes to the treatment of diabetic wounds remains unclear. In this study, the potential therapeutic effects of MLN4924-induced neddylation inhibition on macrophage differentiation and the healing of diabetic wounds were examined both in vitro and in vivo.

Nanoparticles have a wide range of applications in accelerating diabetic wound healing [17–19].Nanoparticles facilitate wound healing and can be used to deliver one or more therapeutic agents such as exosomes growth factors, nucleic acids, antibiotics, and antioxidants so that they can be released continuously in the target tissue [20–22]. Numerous research studies have shown that nanoparticles can significantly enhance the pharmacokinetic characteristics and chemical stability of loaded therapeutics, including small molecule medications, peptides, proteins, small interfering RNA (siRNA), and microRNA (miRNA) [23–25]. Lately, there has been a growing utilization of nanoparticles coated with cell membranes in the field of disease detection and therapy [26,27].This new nanoplatform is distinguished by its ability to avoid phagocytosis, have a longer circulation time, and effectively target specific areas [28]. Macrophage-mimicking nanoparticles possess identical antigenic properties to macrophages and can effectively neutralize endotoxin and proinflammatory cytokines. This method has been employed for the treatment of atherosclerosis, sepsis, and the regeneration of bone tissue [29–31].

The present investigation established a drug transport mechanism utilizing nanospheres coated with macrophage membrane (M-NPs/MLN4924). To inhibit M1 polarization, the nanoparticles' macrophage membranes contain important protein receptors like Tumor necrosis factor receptor 1 (TNFR1), Interleukin-6 receptor (IL-6R), and Toll-like receptor 4 (TLR4). These receptors bind to the inflammatory cytokines (TNF-α, IL-6) and the endotoxin LPS, respectively. Simultaneously, the M-NPs/MLN4924 discharged hindered the polarization of macrophages into the inflammatory M1 type, diminishing superfluous proinflammatory behavior and fostering wound healing. Moreover, the effects of this drug delivery system on endothelial cell proliferation and tube formation were investigated. Under hyperglycemia conditions, M-NPs/MLN4924 induced the growth, movement, and development of vascular endothelial cells, demonstrating similar effects on proliferation, migration, and tube formation. The research offers a two-pronged approach to modulating the immune system for the treatment of wounds in individuals with diabetes. By utilizing a biomimetic membrane system, the levels of toxins were diminished and the inflammatory cytokines were effectively neutralized. The release of MLN4924 by M-NPs/MLN4924 nanoparticles enhanced the growth and formation of tubes in endothelial cells, and at the same time, it suppressed the M1 polarization of macrophages. This suggests that M-NPs/MLN4924 is a promising engineered nanoplatform for promoting the repair of diabetic wounds **(**Scheme 1**B).**

2. Results and discussion

2.1. The proliferation and viability of macrophages are regulated by the neddylation pathway

Delayed healing in diabetic wounds is caused by persistent chronic inflammation resulting from elevated levels of cytokines and the

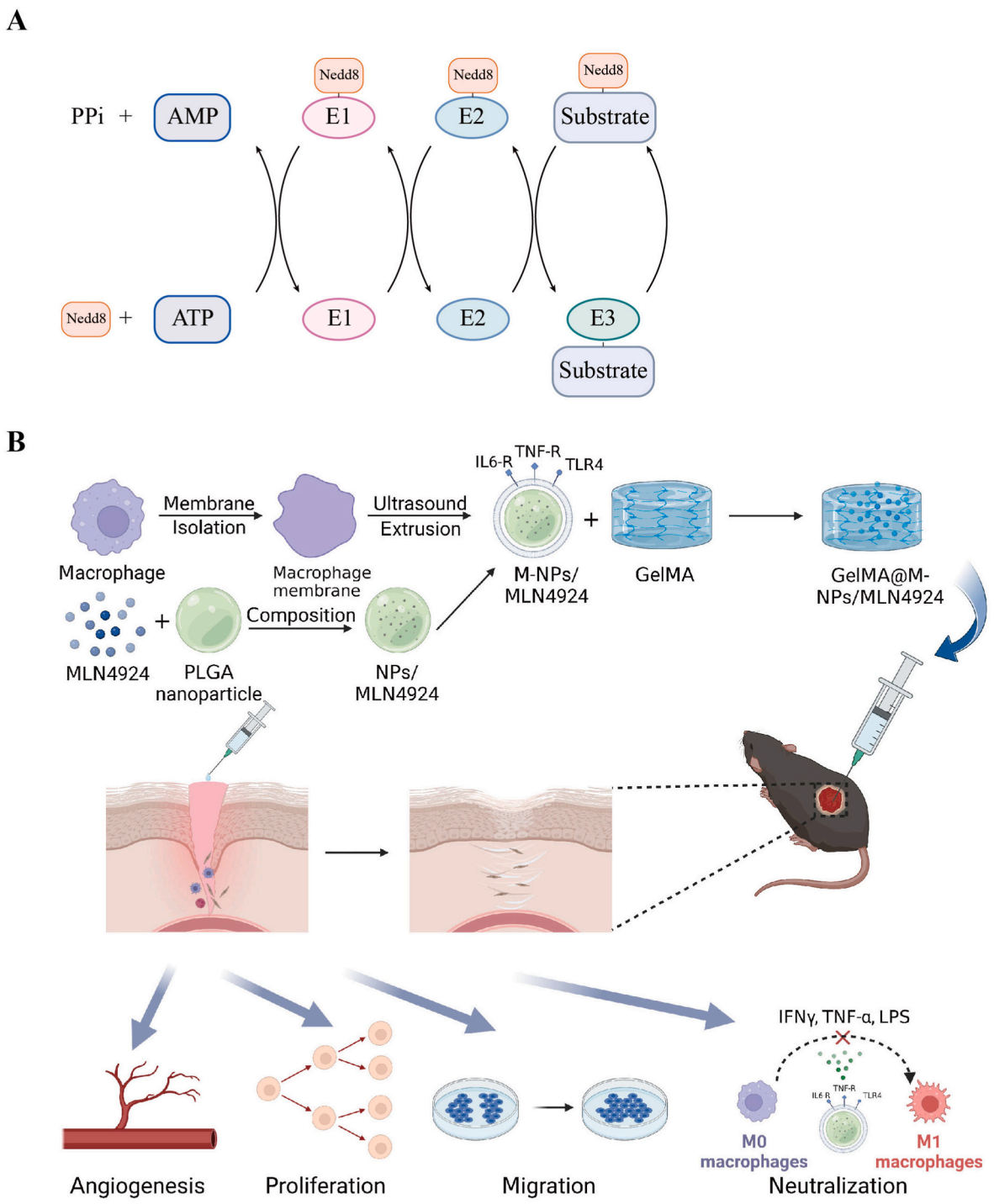

Scheme 1. (A) Schematic illustration of the enzymatic cascades for protein neddylation. The neddylation process involves a series of steps, starting with the activation of NEDD8 by NEDD8 E1 activating enzyme (NAE), then the loading of NEDD8 onto NEDD8-specific E2 conjugating enzyme (UBC12), and ultimately the binding of NEDD8 to protein substrates facilitated by NEDD8 E3 ligase. MLN4924 exerts its inhibitory effect on the neddylation by suppressing the activity of NAE. (B) The diagram depicts the production of M-NPs/MLN4924 and their application in treating diabetic wounds caused by diabetes. The construction of a drug delivery system was achieved by utilizing NPs/MLN4924 coated with macrophage membrane, known as M-NPs/MLN4924, in this research. The nanoparticles regulated endothelial cell proliferation, migration, and angiogenesis while neutralizing inflammatory factors and inhibiting M1 macrophage polarization.

prevalence of M1 macrophages [6]. Consequently, we examined the impact of MLN4924, which partially inhibits neddylation, on the secretion of proinflammatory cytokines by RAW264.7 macrophages at various therapeutic dosages. According to (Fig. 1A), the administration of MLN4924 at concentrations of 0.05 μM, 0. 1 μM, and 0. 2 μM for a duration of 12 h did not exhibit any suppressive impact on the survival of cells. Subsequently, RAW264.7 macrophages were exposed to MLN4924 while being exposed to LPS for 12 h. The findings revealed that MLN4924 could decrease neddylation in RAW264.7 macrophages, as shown in Fig. 1B (top panel). The cullin-RING E3 ligase (CRL) controls the degradation of Inhibitor of NF-κB-alpha (IκBα), an upstream component of NF-κB, which is essential for suppressing NF-κB activity. The current therapy hindered the neddylation process of CRL and stopped the breakdown of IκBα, as shown by the notable buildup of

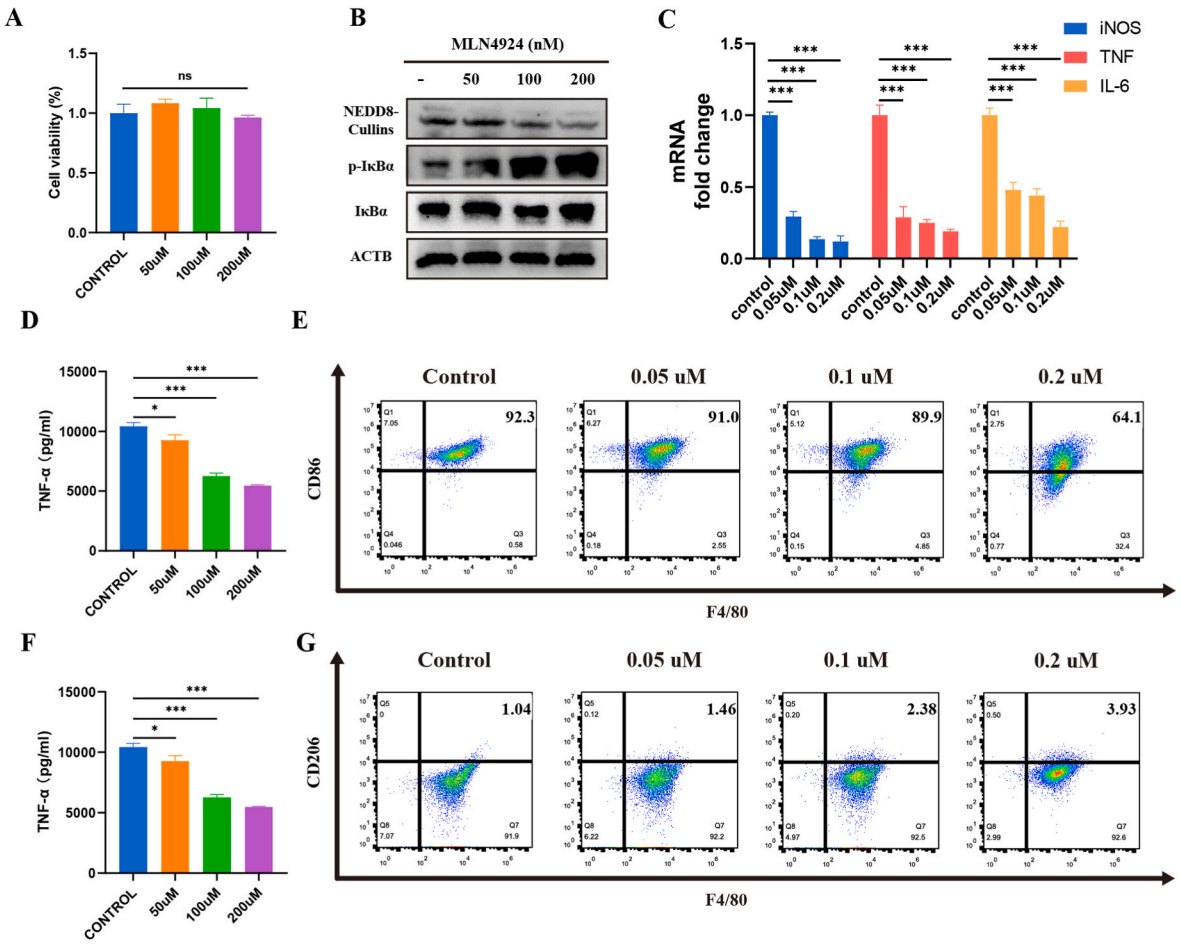

Fig. 1. Attenuation effects of MLN4924 on the inflammatory response of RAW 264.7 cells induced by LPS. (A) After overnight culture, RAW264.7 macrophages were subjected to treatment with MLN4924 at concentrations of 0, 0.05, 0.1, and 0.2 μM for 12 h. Subsequently, cell viability was assessed using the CCK8 assay. (B) Western blots of NEDD8-Cullins, *p*-IκBα, IκBα, and ACTB in MLN4924-treated RAW264.7 macrophages. (C) RT-PCR results of iNOS, IL-6, and TNF-α expression in the RAW264.7 macrophages which were subjected to different treatments. (D, F) ELISA was used to determine the levels of TNF-α and IL-6 cytokines in the supernatant of the cell culture. (E, G) Examples of flow cytometry dot plots showing the results of culturing RAW264.7 macrophages with LPS for 24 h and varying amounts of MLN4924 for another 24 h. The control group was cultured with LPS for 24 h followed by drug-free medium for 24 h. The percentages of F4/80, CD86 and CD206 positive cells. Ns: not statistically significant; *p < 0.05; **p < 0.01; and ***p < 0.001.

phospho-IκBα (*p*-IκBα) (Fig. 1B). Consequently, MLN4924 effectively suppressed the activation of proinflammatory cytokines TNF-α and iNOS in response to LPS stimulation at the mentioned doses (Fig. 1C). Consistently, MLN4924 markedly decreased the concentrations of TNF-α and IL-6 in the supernatant of the cell culture (Fig. 1D–F). Following this, the analysis of flow cytometry revealed a gradual decrease in the count of cells positive for CD86 (M1-type) as the drug concentration increased, while there was a slight increase in the count of cells positive for CD206 (M2-type) (Fig. 1E–G). In line with prior research [16], the findings indicated that the partial hindrance of neddylation alteration impeded the M1 polarization of macrophages and decreased the release of inflammatory cytokines while not impacting the viability of cells.

2.2. *MLN4924 enhances angiogenesis in vitro and ameliorates ROS damage*

Diabetic wound healing failure occurs due to impaired formation of new blood vessels and dysfunction of the cells lining the blood vessels, which are caused by hyperglycemia. Increasing evidence supports the importance of enhancing angiogenesis to accelerate wound healing [32, 33]. Previous research has indicated that hyperglycemia and hyperinsulinemia lead to excessive activation of neddylation, which is associated with diabetic kidney disease and cardiovascular disorders [34, 35].Compared to the control group, hyperglycemia can lead to enhanced neddylation of HUVECs (Fig. 2B, top panel). Similarly, Western blot analysis demonstrates an increase in neddylation in wound skin tissues of diabetic mice (Fig. S1A). The impact of varying MLN4924 concentrations on the proliferation and angiogenesis of Human umbilical vein endothelial cells (HUVEC) was examined. MLN4924 can reduce neddylation in HUVEC cells at doses ranging from 50 to 200 nM (Fig. 2B, top panel). The results from QRT-PCR and western blotting (Fig. 2A and B) indicated that MLN4924 effectively enhanced the expression of the proliferation-associated genes Cyclin D1 and Cyclin D3, which were suppressed by hyperglycemia. MLN4924 significantly enhanced the expression of vascular endothelial growth factor A (VEGF-A) during wound healing induction, in comparison to both the hyperglycemia group and control group. Angiogenesis is significantly influenced by this growth factor, as it can stimulate the multiplication and movement of endothelial cells, thereby playing a crucial part. EdU, a pyrimidine analog of thymidine, can be utilized for the measurement of DNA synthesis in order to identify cellular proliferation. The control group and MLN4924 hyperglycemia group exhibited a higher number of EdU-positive cells compared to the hyperglycemia group, with the 100 nM MLN4924 hyperglycemia group showing the highest count of Edu-positive cells (Fig. 2C–E). The findings suggested that a low dose of MLN4924 exhibited a safeguarding impact on the suppression of HUVEC

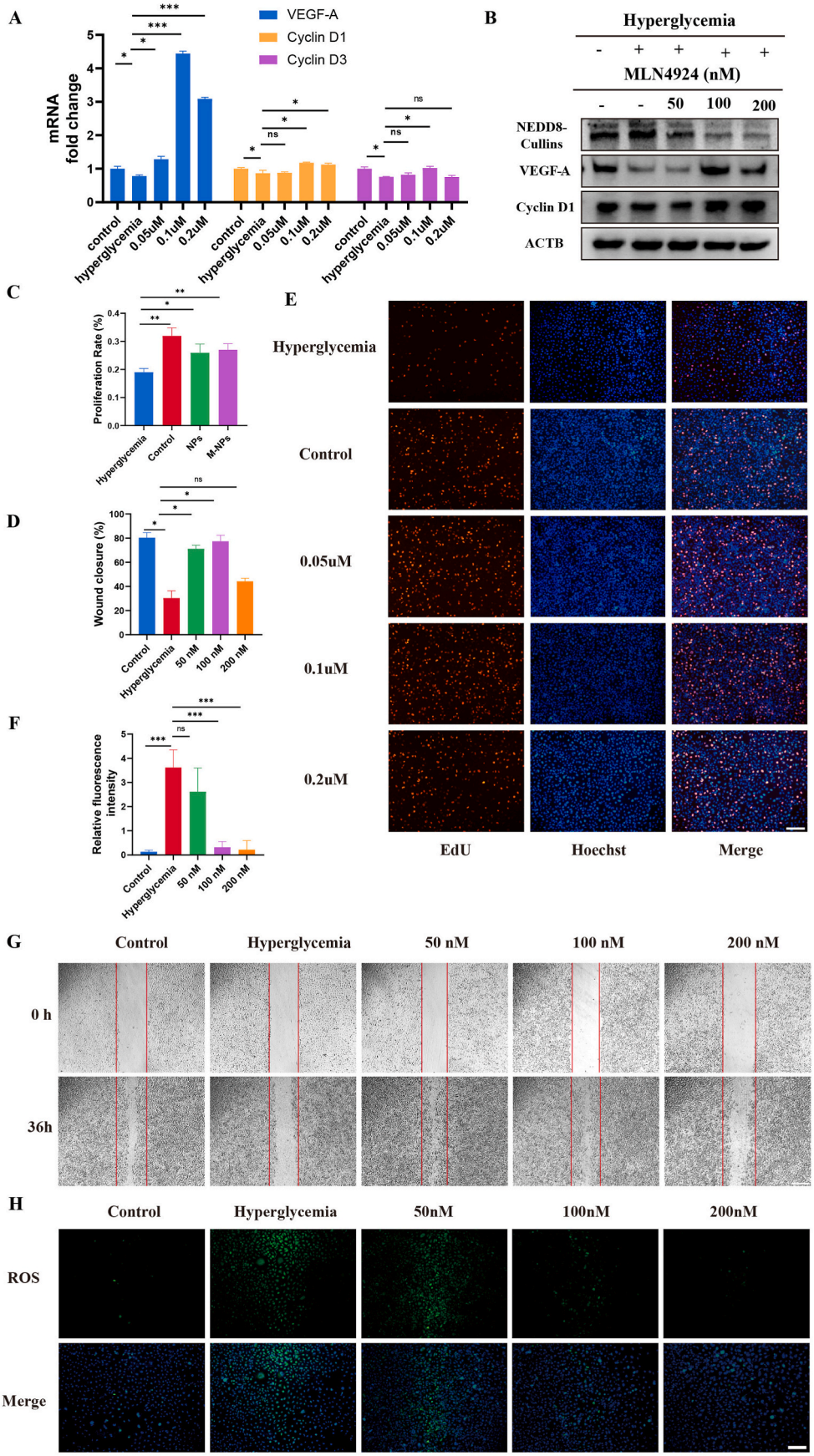

(caption on next page)

Fig. 2. MLN4924 enhances HUVEC function and ameliorates ROS damage in vitro. (A) The effects of different treatments on the expression of VEGF-A, Cyclin D1, and Cyclin D3 in HUVEC were detected by RT-PCR. (B) Western blots of NEDD8-Cullins, VEGF-A, Cyclin D1, and ACTB in HUVECs treated with MLN4924. (C, E) The HUVECs proliferation was assessed using the EdU incorporation assay. Scale bar: 100 μm. (D, G) Conducting an in vitro experiment to assess wound healing on the HUVECs. Scale bar: 50 μm. (F, E) The DCFH-DA was used to evaluate the decrease in ROS levels in HUVECs after various treatments. Scale bar: 100 μm. ns: not statistically significant; *p < 0.05; **p < 0.01; and ***p < 0.001.

function and cellular growth caused by hyperglycemia, with the most effective protection observed at a concentration of 100 nM. Scratch assay was used to investigate the impact of MLN4924 on in vitro wound healing. The findings (Fig. 2D–G) suggested that high blood sugar hindered cell movement in a laboratory setting, whereas a small amount of MLN4924 helped cells transition into the empty area of the plate. The strongest effect was observed for the 100 nM of MLN4924.

ROS damage caused by hyperglycemia is one of the important reasons that diabetic wounds are difficult to heal. It has been shown that MLN4924 has cytoprotective and antioxidant effects on hydrogen peroxide (H2O2) induced damage in cerebellar granule neurons (CGN) [36]. However, its effect on oxidative stress induced by diabetes is still unknown. The ROS indicator, 2′,7′-dichlorodihydrofluorescein diacetate (DCFH-DA), was used to visualize the levels of intracellular ROS. The findings indicated that the cell fluorescence decreased significantly when treated with MLN4924 compared to the control group, and this decrease was dependent on the concentration of MLN4924. Notably, the highest inhibition of oxidative stress was observed at a concentration of 200 nM MLN4924 (Fig. 2F–H).

To sum up, we found that MLN4924 improves the oxidative stress injury induced by hyperglycemia and boosts the growth and movement of HUVECs. However, unlike previous studies, MLN4924 has an optimal concentration for the improvement of endothelial cell function. The strongest promotion effect was observed when the concentration was 100 nM. Additionally, our experiments involving the cultivation of fibroblast cell lines at varying concentrations of MLN4924 revealed that wound healing assays and cell proliferation experiments exhibited the most favorable proliferation and migration levels in fibroblasts at similar concentrations (Fig. S2). As a result, we utilized this ideal concentration to enhance the healing of wounds in diabetic patients.

2.3. Nanoparticle preparation and characterization

The M-NPs/MLN4924 consisted of PLGA nanoparticles loaded with MLN4924, which were then coated with a macrophage membrane. Following the nanoprecipitation method, the PLGA nanospheres with pores were prepared. Subsequently, the macrophage membrane was isolated and coated on the porous PLGA nanospheres through 11 extrusions using an Avanti mini extruder (as shown in Fig. 3A). The encapsulation efficiency (EE) of NPs/MLN4924 nanoparticles is

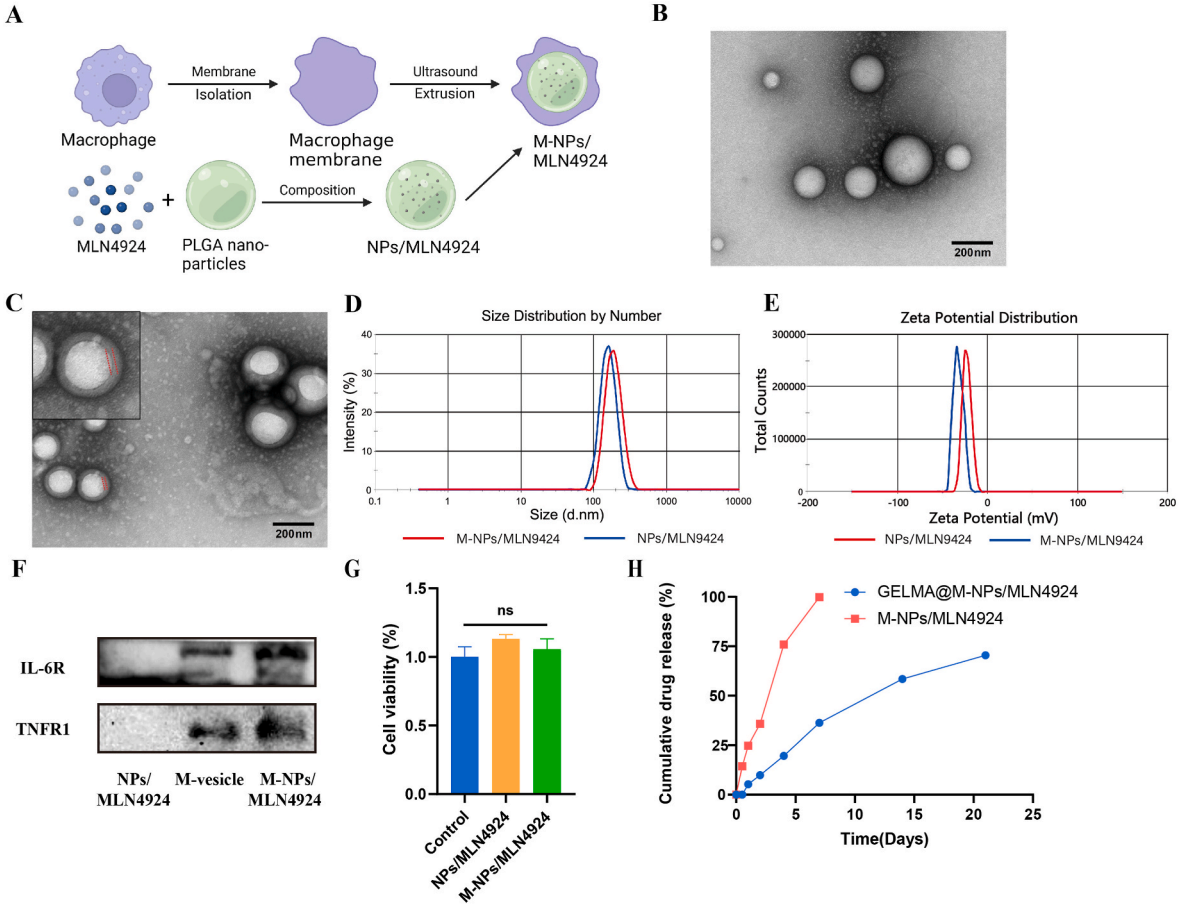

Fig. 3. Investigation of the properties of membrane-coated porous M-NPs/MLN4924 nanospheres. (A) This is a schematic representation of the synthesis process for M-NPs/MLN4924. The TEM images display nanospheres of (B) NPs/MLN4924, and (C) M-NPs/MLN4924. (D) The dimensions and (E) zeta potential of porous NPs/MLN4924 nanospheres and M-NPs/MLN4924. (F) Western blots were performed on NPs/MLN4924 and M-NPs/MLN4924 to detect TNFR1 and IL-6R. (G) Biocompatibility was assessed by performing a CCK-8 assay after 24 h of cultivation (*P < 0.05 when compared to the control). (H) The release of MLN4924 from M-NPs/MLN4924 and GelMA@M-NPs/MLN4924 was observed in PBS at 37 °C and pH 7.4 for a duration of 21 days.

approximately 95 %, while the drug loading capacity (DLC) is about 10 %. The transmission electron microscope (TEM) images showed the NPs exhibited predominantly spherical shapes with a mean particle size of approximately 150–200 nm (Fig. 3B) and a thin uniform coating on the surface of M-NPs/MLN4924 (Fig. 3C). This result shows that there is a single-layer coating on M-NPs/MLN4924 nanoparticles. Based on dynamic light scattering (DLS), the diameter of the fused nanoparticles increased from 167 to 189 nm (Fig. 3D). On M-NPs/MLN4924 nanospheres, this corresponds to a macrophage membrane thickness of about 11 nm. Furthermore, the zeta potential of the membrane surface decreased from −23.50 ± 3.6 mV to −30.27 ± 3.2 mV (Fig. 3E). All these results revealed the successful synthesis of membrane vesicles with PLGA nanospheres. Western blotting was used to analyze the membrane surface marker proteins, IL-6R and TNFR1, which interacted with the pro-inflammatory cytokines IL-6 and TNF-α, correspondingly. As shown in (Fig. 3F), these proteins were expressed on both macrophage membranes and M-NPs/MLN4924. To evaluate the cytotoxic effects of M-NPs/MLN4924 and PLGA-coated MLN4924 nanoparticles (NPs/MLN4924), a CCK-8 kit from Beyotime in China was utilized. The results from Fig. 3G indicated that these nanoparticles did not exhibit noteworthy cytotoxicity when administered at therapeutic doses during the experiment. As shown in the in vitro release curves of drug nanoparticles (Fig. 3H), MLN4924 could be continuously released from M-NPs/MLN4924 and GelMA@M-NPs/MLN4924. After loading the final M-NPs/MLN4924 into the porous GelMA hydrogel, the sustained release effect lasted longer, showing its potential for long-term therapeutic effect. Collectively, these findings revealed that M-NPs/MLN4924 nanospheres retain the macrophage membrane structure with its key proteins, thereby providing functions to enhance drug delivery, reduce toxin levels, and neutralize inflammatory factors.

2.4. The in vitro inhibition of inflammation by nanoparticles

In the previous section (Results 2.3), we identified the optimal drug concentration that can both inhibit macrophage polarization and inflammatory cytokine secretion, and promote HUVEC proliferation and migration. HUVEC cells were co-cultured with classically activated M1 macrophages to simulate the high-glucose and inflammatory environment of the diabetic wound (Fig. 4A). In this co-culture environment, we further investigated the effect of macrophage membrane nanoparticles on macrophage function. The ELISA findings (Fig. 4B, C) indicated that the secretion quantities of TNF-α and IL-6 in RAW264.7 macrophages were notably reduced in both the NPs/MLN4924 and M-NPs/MLN4924 groups compared to the control group. The M-NPs/MLN4924 group had the lowest number, with TNF-α and IL-6 secretion levels being only 50 % and 33 % of the control group, respectively. In the M-NPs/MLN4924 group, the qPCR results (Fig. 4D) showed the lowest mRNA expression levels for the TNF-α, IL-6, and iNOS genes. Flow cytometry analysis showed (Fig. 4E and F; Fig. S1B and C) that compared with the control group, $CD86^{+}$ (M1-type) macrophages were less than 75 % in the NPs/MLN4924 group and only 61.4 % in the M-NPs/MLN4924 group, which significantly inhibited the LPS-induced M1 polarization. The results suggested that the sustained release of MLN4924 from PLGA nanoparticles could inhibit the M1 polarization of RAW264.7 macrophages and reduce the expression and secretion of pro-inflammatory cytokines, while the biomimetic membrane system further reduced inflammatory cytokines levels and neutralized them.

2.5. Human umbilical vein endothelial cells proliferation, migration, and angiogenesis induced by nanoparticles

We further evaluated the effects of M-NPs/MLN4924 on HUVEC proliferation, migration, and angiogenesis. The proliferation of HUVECs

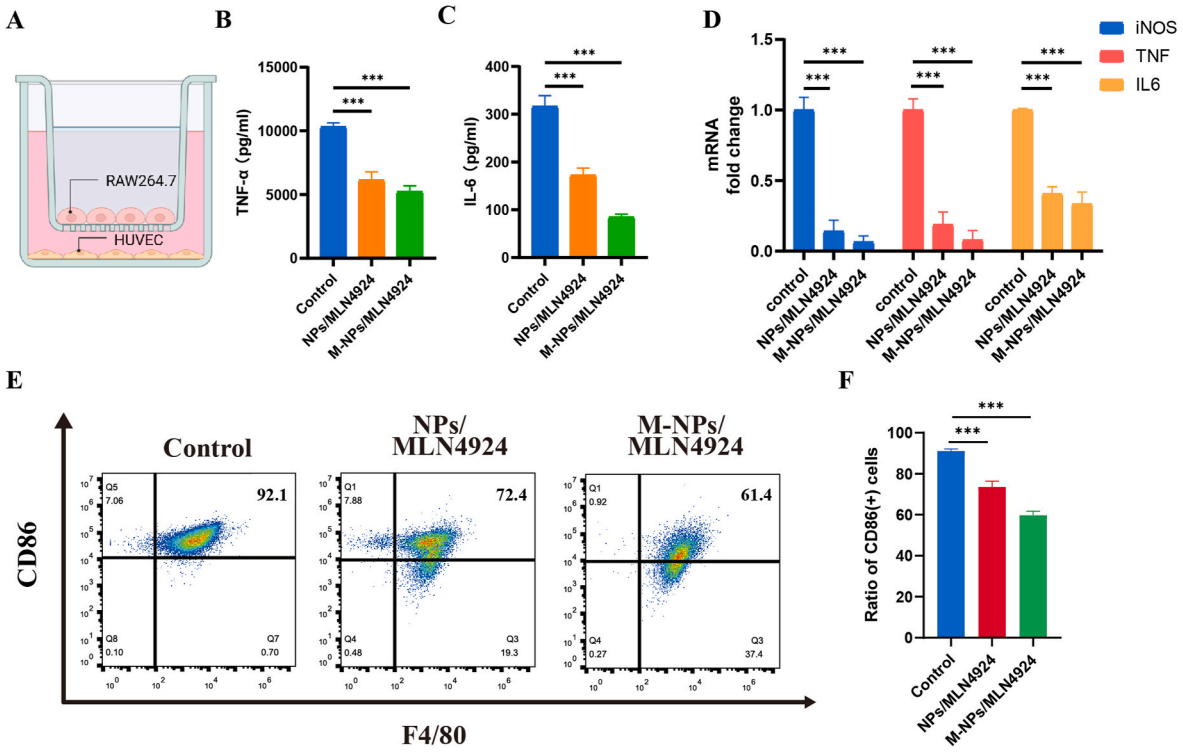

Fig. 4. M-NPs/MLN4924 can inhibit inflammation, reduce ROS damage, and enhance HUVEC function. (A) HUVECs were co-cultured with classically activated M1-type macrophages. (B, C) ELISA was used to determine the levels of TNF-α and IL-6 in the supernatant of the cell culture. (D) RAW 264.7 cells were stimulated with LPS for 24 h and subjected to various treatments, and the expression of iNOS, IL-6, and TNF-α was determined using RT-PCR. (E, F) The FACS histogram depicted the flow cytometry findings of RAW264.7 macrophages that were cultured for 24 h with LPS and then with various treatments for 24 h, with or without NPs/MLN4924 and M-NPs/MLN4924. The results show the proportions of cells expressing CD86; *p < 0.05; **p < 0.01; and ***p < 0.001.

was detected by EdU incorporation and calcein-AM staining (Fig. 5A, B, I, J). NPs/MLN4924 and M-NPs/MLN4924 were co-cultured with HUVECs for 1 and 3 days, and cell morphology was analyzed by calcein-AM staining. The findings showed that both NPs/MLN4924 and M-NPs/MLN4924 enhanced cellular growth, with M-NPs/MLN4924 resulting in the most significant increase in cell proliferation. The control group and the nanoparticle treatment group had a higher number of EdU positive cells compared to the hyperglycemia group, with the M-NPs/MLN4924 group showing the highest count of EdU positive cells. In order to assess the impact of nanoparticles on the movement of HUVECs, we conducted both a transwell migration assay and a wound healing assay. The findings indicated that both NPs/MLN4924 and M-NPs/MLN4924 enhanced the speed of HUVEC movements, which were initially suppressed by hyperglycemia. The wound healing assay results (Fig. 5C–F) showed that the wound closure in the high glucose group was significantly lower compared to the other three groups. The wound healing in the NPs/MLN4924 group was comparable to that in the control group. M-NPs/MLN4924 group showed the strongest promoting effect on wound healing. Compared with the hyperglycemia group, HUVECs in the M-NPs/MLN4924 group showed the fastest cell migration and about 2 times the wound healing rate compared to the hyperglycemia group. Furthermore, the transwell findings (Fig. 5E–G) indicated a notable increase in cell numbers for both the NPs/MLN4924 and M-NPs/MLN4924 groups compared to the control and hyperglycemia groups. Moreover, the M-NPs/MLN4924 group exhibited approximately threefold higher cell counts than the hyperglycemia group. The repair of traumatic tissue defects heavily relies on angiogenesis. HUVECs were subjected to a tube formation assay using Matrigel to evaluate the development of capillary networks. Under hyperglycemia conditions, it was observed that NPs/MLN4924 and M-NPs/MLN4924 augmented the tube formation capacity of HUVECs. Notably, M-NPs/MLN4924 exhibited the most significant enhancement in tube formation, as depicted in Fig. 5D–H. In summary, the above in vitro results revealed the dual effects of M-NPs/MLN4924 on macrophages and HUVEC cells. In the presence of hyperglycemia, it has a notable ability to suppress macrophage polarization and the release of inflammatory substances, while enhancing the growth, movement, and formation of tubes by HUVECs.

2.6. GelMA@M-NPs/MLN4924 enhanced the rate of wound closure, repaired the epithelial tissue, and promoted the formation of granulation tissue in mice with diabetes

The process of wound healing is intricate and consists of various stages including inflammation, proliferation, and remodeling. It requires the involvement of numerous cells, growth factors, and extracellular mesenchyme. Diabetic wounds often suffer from poor wound healing, bacterial infection, vascular lesions, and oxidative damage, leading to chronic ulcers [37,38]. GelMA hydrogel has been used as a tissue repair material by many researchers due to its superior biocompatibility, antibacterial ability, degradability, and mechanical properties [39,40]. The porous GelMA with reticular pores size of 100–200 μm is advantageous to cell proliferation by providing the 3D network for cell adhesion and effective transport of nutrients [41]. The swelling curve of the hydrogel exhibited a marked increase in swelling ratio during the first 2 h followed by a plateau (Fig. S3A), while the degradation curve showed a gradual degradation trend (Fig. S3B). We added **M-NPs/MLN4924** to the porous GelMA hydrogel during hydrogel formation (Fig. 6A). The transmission electron microscope (TEM) images revealed that the pore size of the porous hydrogel remained unchanged before and after loading of the nanoparticles (approximately 100–200 μm) (Figs. S3C and D). To evaluate the efficacy of M-NPs/MLN4924 on diabetic wound healing, we established a mouse model of chronic diabetic wounds and the hydrogel of each group was applied around the wound by injection. The results showed that both GelMA@NPs/MLN4924 and GelMA@M-NPs/MLN4924 accelerated wound closure compared with the hyperglycemia group. GelMA@M-NPs/MLN4924 had the best results at 3, 10, and 14 days after surgery (Fig. 6B and C). Small animal doppler examination showed that both GelMA@NPs/MLN4924 and GelMA@M-NPs/MLN4924 could significantly enhance wound blood flow, among which GelMA@M-NPs/MLN4924 had the greatest effect (Fig. 6D and E).

Evaluation of the development of fresh epithelial and granulation tissue using HE staining demonstrated the degree of granulation tissue formation was significantly higher in GelMA@M-NPs/MLN4924-treated diabetic wounds when compared to hyperglycemia groups (Fig. 7A–F). Masson's trichrome staining showed more extensive collagen deposition in the GelMA@M-NPs/MLN4924 group, indicating that GelMA@M-NPs/MLN4924 had superior ECM remodeling capacity (Fig. 7B–E). The thickness of granulation tissue and collagen deposition in the GelMA@NPs/MLN4924 group were higher than in the hyperglycemic group, but lower than those in the GelMA@M-NPs/MLN4924 group and the control group. Immunohistochemistry (IHC) of CD31, a marker of vascular endothelial cells, was used to analyze microvascular density. In comparison to the high-glucose group, the GelMA@M-NPs/MLN4924 and GelMA@NPs/MLN4924 groups exhibited increased CD31 expression, indicating an amelioration of angiogenesis in diabetic wound healing (Fig. 7C and D). The Western blot results revealed higher levels of neddylation in the hyperglycemia and GelMA groups, whereas the GelMA@M-NPs/MLN4924 and GelMA@NPs/MLN4924 groups exhibited reduced neddylation and enhanced expression of VEGF-A protein (Fig. S5). These results suggest that GelMA@M-NPs/MLN4924 promotes angiogenesis and collagen synthesis in the wound area and accelerates diabetic wound healing.

2.7. GelMA@M-NPs/MLN4924 hydrogel reduced inflammation and ROS levels

In order to further examine the potential of GelMA@M-NPs/MLN4924 hydrogels in reducing oxidative stress and inflammation caused by diabetic trauma in mice, we conducted an analysis of intracellular inflammation and ROS levels in vivo using immunofluorescence staining and dihydroethidium (DHE) staining (Fig. 8A–E). Samples of wounds were gathered on days 3, 7, and 14 to undergo DHE staining. On day 3 (Fig. 8B), the findings indicated that the levels of ROS in the hyperglycemia group and GelMA group were notably higher compared to the control group, GelMA@M-NPs/MLN4924 group, and GelMA@M-NPs/MLN4924 group, which exhibited significantly lower ROS levels. Following that, the differences mentioned earlier were gradually diminished on days 7 and 14. However, the levels of ROS in the hyperglycemia and GelMA groups remained elevated compared to the other three groups (Fig. 8C and D). Excessive oxidative stress and decreased antioxidant capacity of tissues lead to redox imbalance, which is one of the main reasons for nonhealing diabetic wounds [42]. MLN4924 has been shown to prevent oxidative stress by the accumulation of nuclear factor-erythroid 2 related factor 2 (Nrf2) protein, a vital transcription factor regulating the cellular response to oxidative stress [36,43]. Polarization of macrophage activation phenotype (M1 or M2) was analyzed by evaluating the levels of inducible nitric oxide synthase (iNOS) (M1 indicator) and arginase 1 (Arg1) (M2 indicator). Immunofluorescence staining for ARG1 and iNOS on skin sections revealed that iNOS expression was significantly lower and ARG1 fluorescence intensity was significantly higher in the GelMA@M-NPs/MLN4924 group compared to the hyperglycemia group. The results indicate that consistent with in vivo experiments, the PLGA nanoparticles loaded with MLN4924 and the biomimetic membrane system significantly suppressed inflammation in diabetic mouse wounds, inhibited macrophage M1 polarization, and promoted their transition to the M2 reparative phenotype (Fig. 8E, F, G). For a recent example, a study showed that MLN4924 inhibits ROS production by blocking the NF-κB inflammatory pathway, which is consistent with our observations [44]. Finally, we evaluated the biocompatibility of the drug delivery platform. H&E staining of the major organs of healthy mice on the 14th day after

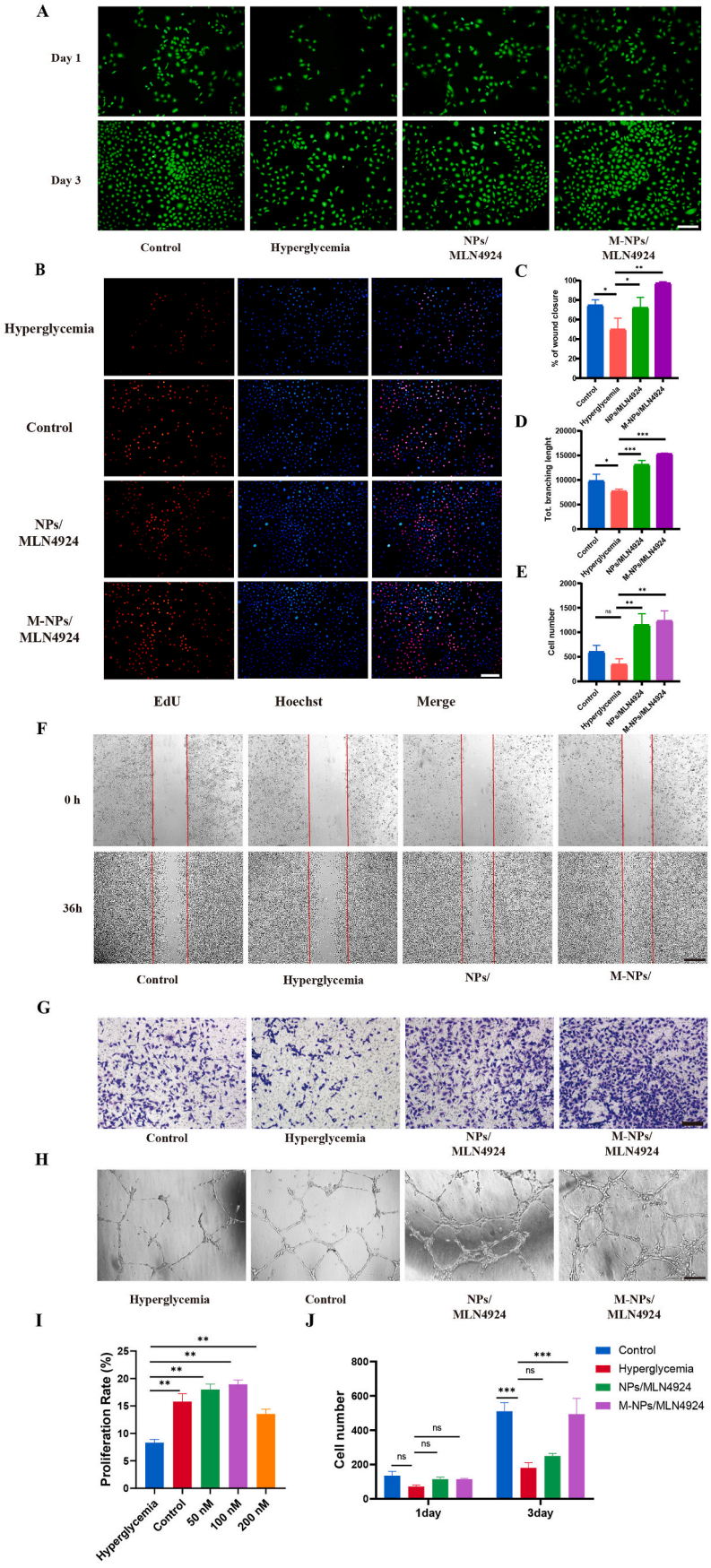

(caption on next page)

Fig. 5. Cell proliferation, migration, and angiogenesis were enhanced by M-NPs/MLN4924. (A, J) The proliferation of HUVECs was observed by calcein-AM staining on days 1 and 3. Scale bar: 100 μm.Scale bar: 100 μm. (B, I) HUVECs proliferation was assessed using the EdU incorporation assay. Scale bar: 100 μm. (C, F) The wound healing rate of each group was quantitatively evaluated by HUVECs in vitro. Scale bar: 100 μm. (D, H) The assessment of tube formation in the four categories. (E, G) To measure the migratory capacity of HUVECs following different treatments, a transwell assay was utilized. Scale bar: 100 μm ns not statistically significant; *p < 0.05; **p < 0.01; and ***p < 0.001.

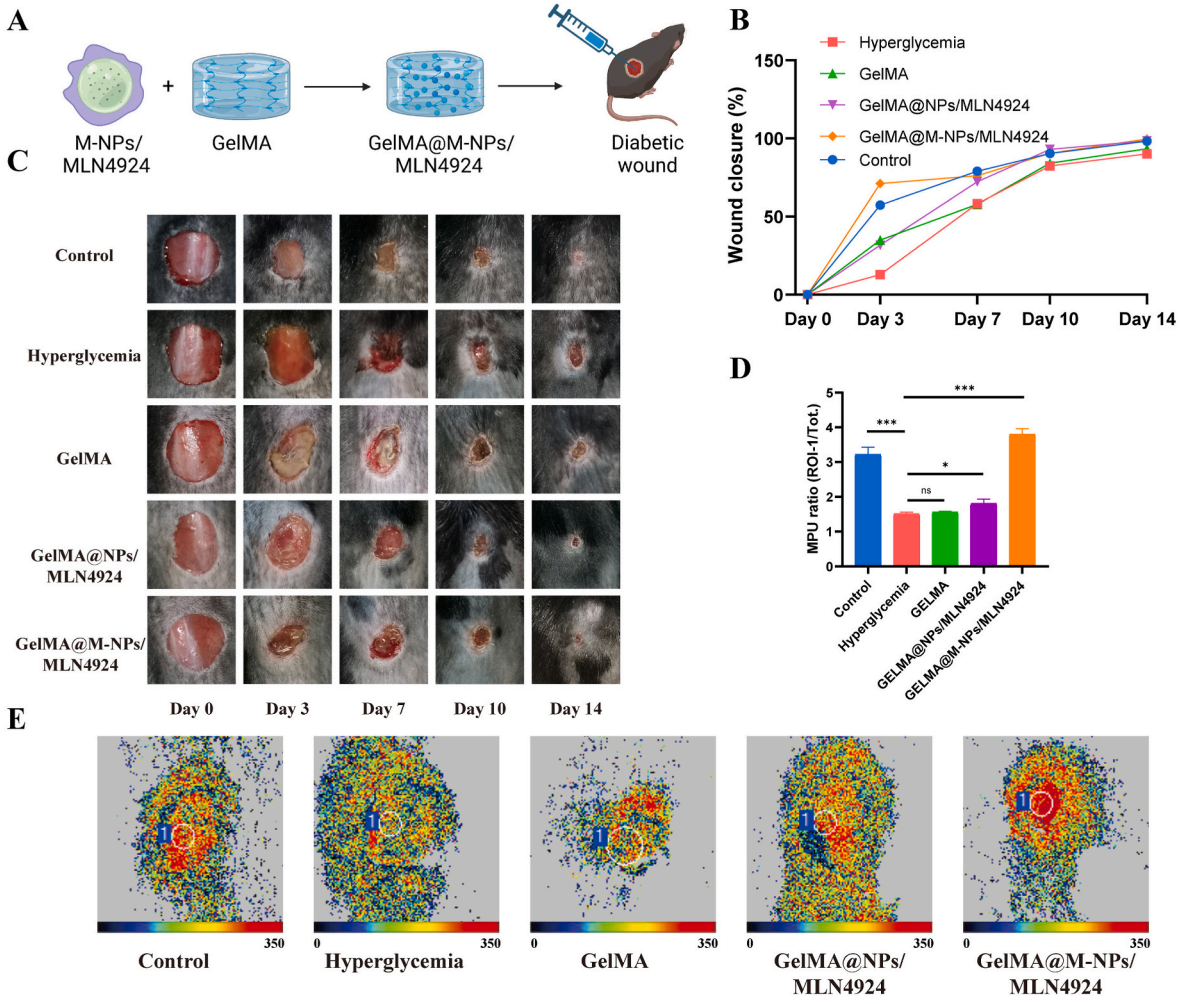

Fig. 6. GelMA@M-NPs/MLN4924 accelerated diabetic wound healing in vivo. (A) The hydrogel mixed with nanoparticles is applied to the diabetic wound by injection. (B) Illustrative pictures showing full-thickness injuries in diabetic rats on days 0, 3, 7, 10, and 14 post-administration of PBS (Control), GelMA, GelMA@NPs/MLN4924, and GelMA@M-NPs/MLN4924. (C) The closure rates of wound healing in each group were computed through the utilization of the ImageJ software. (D, E) Small animal doppler examination was used to evaluate the blood perfusion of wounds. The blood perfusion results are displayed as the proportion of the wound area (ROI-1) to the overall area (Tot).

different treatments showed no significant tissue damage in the treated groups compared to the control group, indicating the excellent biocompatibility of GelMA@M-NPs/mln4924 (Fig. S6). In conclusion, GelMA@M-NPs/MLN4924 hydrogel showed excellent performance in vivo, which significantly promoted wound healing, vascular growth, anti-inflammation and anti-oxidative stress in diabetic mice.

3. Conclusion

Currently, medicine faces a significant obstacle in diabetic foot ulcers. Neddylation, a post-translational modification of proteins, plays a crucial role in governing numerous biological processes through its impact on the subcellular distribution, stability, validation, and functionality of target proteins [45]. The current investigation discovered that MLN4924, by partially inhibiting neddylation, hindered the production of proinflammatory cytokines in macrophages induced by LPS. This effect primarily resulted from the accumulation of IκB-α, which inhibited NF-κB activity. Furthermore, at the same concentration, MLN4924 notably enhanced the migration, proliferation, and tube formation of HUVEC, and also exhibited excellent performance under a hyperglycemia environment for wound healing.

In our research, we present a drug delivery system that mimics macrophages, where NPs/MLN4924 is covered with cell membranes from macrophages. Macrophage membrane-coated nanoparticles can efficiently capture and sequester various proinflammatory cytokines and chemokines, crucial for neutralizing inflammation during diabetic wound healing, due to the existence of membrane antigens like TNFR1 and IL-6R on macrophages. To summarize, M-NPs/MLN4924 hydrogel showed great potential for accelerating diabetic wound healing. The microenvironment of diabetic wounds is oxidative and M1-polarized, and the M-NPs/MLN4924 hydrogel synergistically ameliorates ROS damage, induces angiogenesis, enhances proliferation, forms

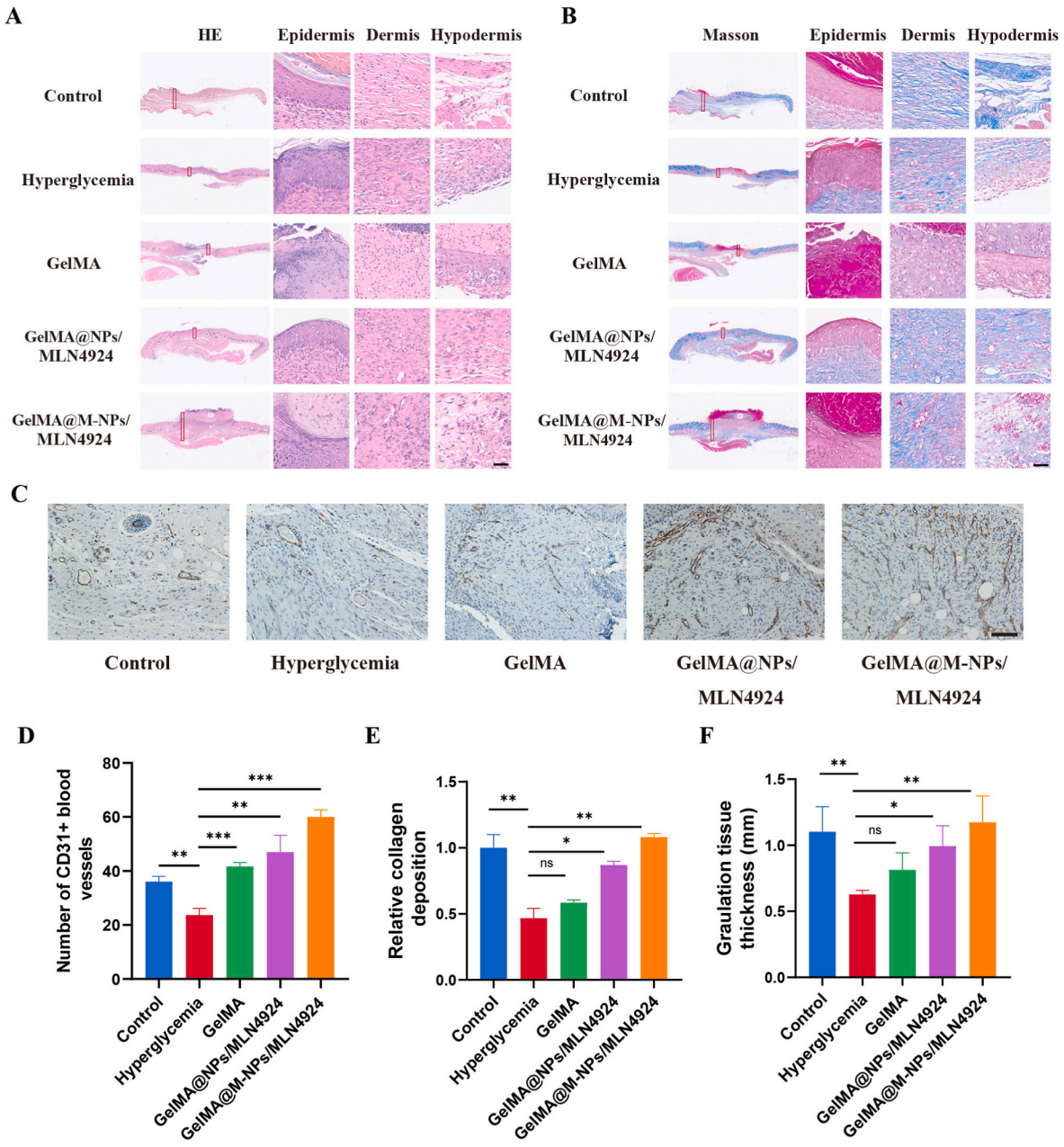

Fig. 7. GelMA@M-NPs/MLN4924 accelerated diabetic wound healing in vivo. Evaluation of wound regeneration on the 14th day after injury was assessed using (A) H&E and (B) Masson's trichrome staining for various treatments. Scale bar: 50 μm. (C) Immunohistochemical analysis images of CD31 expression in the wound tissue. Scale bar: 100 μm. (D) The number of CD31 positive areas was quantified among the various groups. The statistical results of Masson's trichrome (E) and H&E staining (F). ns not statistically significant; *$p < 0.05$; **$p < 0.01$; and ***$p < 0.001$.

granulation tissue and collagen accumulation, thus showing great potential to promote diabetic skin remodeling in vivo. Therefore, the M-NPs/MLN4924 hydrogel represents a multifunctional therapeutic approach, which can effectively facilitate tissue regeneration while concurrently mitigating the presence of inflammation.

4. Experimental section/methods

Cell culture: The human umbilical vein endothelial cell line HUVEC, L929 mouse fibroblast cell lines and the RAW264.7 cell line derived from mouse macrophages were acquired from the Cell Bank of the Chinese Academy of Science in Shanghai, China. These cell lines were maintained in a complete medium supplemented with 10 % fetal bovine serum (FBS) obtained from Gibco in the United States. In order to replicate hyperglycemic conditions in a laboratory setting, HUVECs were exposed to D-(+)-Glucose (Sigma-Aldrich, USA) at a concentration of 35 mmol/l. The experimental group (exp) received a treatment of 5.6 mmol/l glucose.

Macrophage collection and cell membrane derivation: Cell membranes were extracted from RAW264.7 cells using a membrane protein extraction kit (Beyotime, China). Initially, the cells were submerged in a refrigerated solution for extracting membrane proteins for a duration of 15 min. Next, the cells were moderately broken down 10 to 20 times using a Dounce homogenizer. Low-speed centrifugation (800×*g*, 10 min) was used to remove nuclei and a small amount of intact cells, while high-speed centrifugation (15,000×*g*, 30 min) was performed to obtain cell membrane precipitates. Membrane protein content was measured using the BCA method. The cell membrane was applied for 15 min using

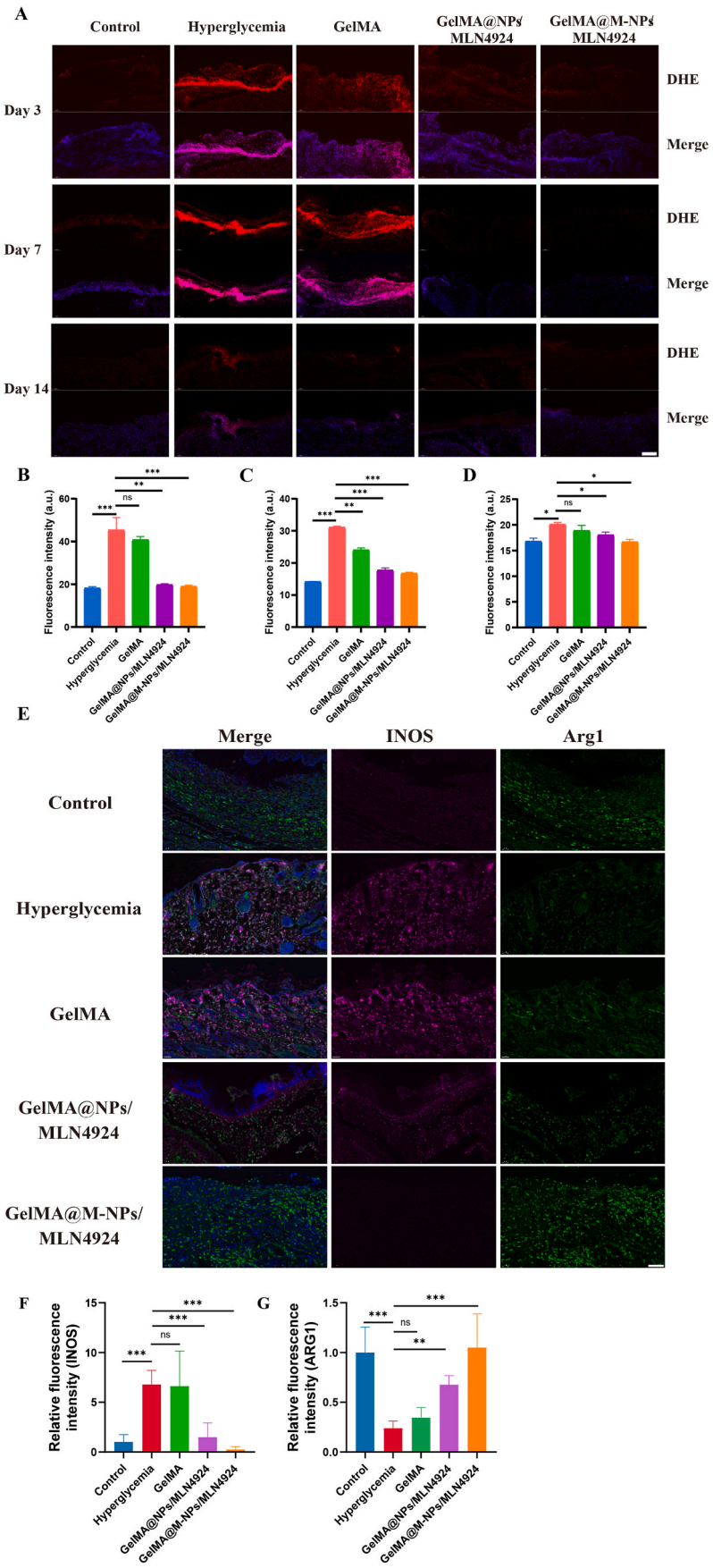

(caption on next page)

Fig. 8. GelMA@M-NPs/MLN4924 ameliorates ROS production in mice.
(A) ROS levels in the wound site were assessed using dihydroethidium (DHE) after applying various treatments. Scale bar: 200 μm. (B–D) DHE fluorescence was used to determine the decrease in ROS levels following treatment with PBS (Con), GelMA, GelMA@NPs/MLN4924, and GelMA@M-NPs/MLN4924. (E–G) Immunofluorescence staining was used to detect the expressions of Arg1 and iNOS in skin tissue of different groups after 14 days. Scale bar: 100 μm. Differences were assessed using one-way ANOVA, followed by a Tukey post hoc test for pairwise comparison. The data was presented as mean ± SD, with statistical significance denoted as ****$p < 0.0001$, ***$p < 0.001$, **$p < 0.01$, *$p < 0.05$.

an ultrasonic bath. In the end, macrophage membrane vesicles were acquired through 11 extrusions utilizing an Avanti mini extruder equipped with 400 nm polycarbonate porous membranes from Avanti in Canada.

Synthesis and characterization of nanoparticles: The PLGA core was formed by nanoprecipitation using a carboxy-terminal 50:50 polylactic acid-glycolic acid copolymer (LAP, USA) as the material. Following the dissolution of PLGA in acetone at a concentration of 10 mg/mL, a swift addition of 1 mL of the PLGA solution to 2 mL of deionized water was made, and subsequently, the mixture was subjected to a vacuum to eliminate the acetone. MLN4924-loaded nanoparticles were created by incorporating 10 % (w/w) MLN4924 (purchased from MCE, China) into the PLGA core synthesis.

To finish the membrane coating, the fusion of macrophage membranes with NPs/MLN4924 was achieved through a mini-extruder for a minimum of 20 times. Additionally, an ultrasound bath operating at a frequency of 40 kHz and a power of 100 W was utilized for a duration of 2 min. Pure M-NPs/MLN4924 were obtained after multiple washes with PBS. Western blotting was used to determine the specific surface markers on macrophage membranes, NPs/MLN4924, and M-NPs/MLN4924. After staining with 1 % uranyl acetate, the transmission electron microscope (Tecnai G2 20, FEI, USA) was used to observe the morphology of the NPs/MLN4924 and M-NPs/MLN4924. Using a Malvern Zetasizer (Nano ZS, Malvern, U. K.), the NPs/MLN4924 and M-NPs/MLN4924 were analyzed for their size distribution and ζ potential.

A certain mass of GelMA@M-NPs/MLN4924 hydrogel (10 mg/g) and M-NPs/MLN4924 (10 mg) were weighed and placed in a dialysis bag (5000Da). Each group was immersed in a beaker containing 1 L of PBS solution and shaken at 37 °C (100 rpm). At the set time points (namely 6, 12, 24, 48, 96 h, 7, 14, and 21 days), the dialysis bag was removed from the beaker, and 10 mL of release medium solution was precisely aspirated (blank PBS was filled back into the dissolution cylinder). The aforementioned medium solution was dried by evaporation, followed by the addition of 0.5 mL of pure ethanol and complete dissolution. Subsequently, the supernatant was obtained through high-speed centrifugation at 10000 rpm for 30 min. After filtration, MLN9424 was detected by liquid chromatography (HPLC), and the drug release rate in each group was calculated. To determine the encapsulation efficiency (EE) and drug loading capacity (DLC) of NPs/MLN4924 and M-NPs/MLN4924 were calculated using the following formulas:

$$EE(\%) = \frac{MLN4924\ encapsulated\ in\ M-NPs}{total\ MLN4924} \times 100\%$$

$$DLC(\%) = \frac{MLN4924\ encapsulated\ in\ M-NPs}{weight\ of\ MLN4924} \times 100\%$$

Synthesis of hydrogels: The porous GelMA (EFL, China) was dissolved in PBS at 37 °C and then filtered using a 0.22 μm filter. By employing magnetic stirring, the solution was thoroughly mixed after the addition of the nanoparticles. The composite hydrogel was obtained after 15s photo-crosslinking by 405 nm blue laser radiation.

Swelling/degradation ratio of GelMA hydrogel: The GelMA hydrogel (300 μl) was placed onto cell culture dishes, and then soaked in PBS for 24 h. After removing the surface water, the swelling samples were weighed at specific time intervals (0.5/1/2/6/12/24 h). The swelling ratio was calculated using the formula: swelling ratio = (Wt − Wd)/Wd × 100 %, where Wd represented the dry weight of the hydrogel, and Wt represented the swollen weight of the hydrogel. We also assessed the degradation of the hydrogel at specific time points (day 2, 5, 7, 8, 14, 21). The weight of the hydrogel was measured after removing the surface supernatant, and the degradation ratio was calculated using the formula: degradation ratio = W1/W0 × 100 %, where W0 represented the initial wet weight of the hydrogel, and W1 represented the wet weight of the hydrogel at a given time point.

Cell safety evaluation: Assessment of cell safety involved the use of the CCK-8 kit (Beyotime, China) to detect cell viability. HUVECs were placed in 24-well dishes with a density of 5 × 105 per well and exposed to various MLN4924 concentrations for specified durations. Afterwards, the cells were incubated in a solution with 10 % CCK-8 for 2 h at a temperature of 37 °C. A microplate reader was used to measure the absorbance of the samples at a wavelength of 450 nm (BioTek, USA).

ELISA: Following a 24-h incubation period with various treatments, the culture medium was gathered from 24-well plates in the diverse groups and subsequently subjected to centrifugation. ELISA kits (Boster, China) were used to detect cytokine levels (TNF-α and IL-6) in the supernatant, as per the guidelines provided by the manufacturer.

Characterization of membrane proteins: Analysis of membrane proteins involved isolating membrane proteins from LPS-induced RAW 264.7 macrophages through the utilization of a membrane protein extraction kit (Beyotime, China) following the guidelines provided by the manufacturer. Western blotting was used to detect the presence of numerous membrane surface proteins, including TNFR1 and IL-6R.

Flow cytometry: RAW 264.7 cells were induced to differentiate into the M1 phenotype by LPS (100 ng/mL) for 24 h. Subsequently, they were further cultured for 24 h using PBS (Control) and other different treatments. After treatment and culture for 24 h in each group, RAW 264.7 was scraped off, washed, and sub-packed into flow tubes. Blocking was performed with blocking buffer (Biolegend, USA) for 15 min, followed by allophycocyanin (APC) conjugated anti-CD86 antibody (1:100, BioLegend, USA), PE-conjugated anti-F4/80 antibody (1: 100, BioLegend, USA) and FITC conjugated anti-CD206 antibody (1:100, BioLegend, USA) for 1 h. Cells were analyzed using a BD flow cytometer with FlowJo software.

Wound healing assay: In the wound healing experiment, HUVECs were enzymatically digested and then placed in six-well plates. Once the cell culture reached 90 % confluence, a sterile 200 μl micropipette tip was used to create a perpendicular scratch on the well plate. The liquid in the cell culture was removed, and the plates in the wells were rinsed three times using PBS. Photographs were taken at regular intervals to document the addition of serum-free medium. ImageJ (Media Cybernetics, USA) was utilized to evaluate the extent of wound closure.

Tube formation assay: The formation of capillary networks by HUVEC was assessed using the tube formation assay in Matrigel (Corning, USA). After different treatments, cells were seeded in 96-well Matrigel-coated plates and incubated at 37 °C for 6 h. The formation of capillary-like structures was observed by a light microscope (Olympus, Japan) and ImageJ (Media Cybernetics, USA) was used to count the number of capillaries formed.

EdU incorporation assay: Cell proliferation was observed through the EdU (5-ethynyl-2′-deoxyuridine) incorporation assay. The cells were treated with EdU for a duration of 2 h and subsequently immobilized using 4 % PFA. The HUVECs were stained using an EdU incorporation assay following the guidelines provided by the manufacturer.

Transwell assay: Migration assays were performed using 24-well Transwell chambers equipped with filters of 8 μm pore size (Corning, USA). HUVECs cultured in medium without serum were placed in the upper chamber, while the lower chamber was filled with complete

medium. Following a 24-h period, the cells situated at the filter's upper section were eliminated by delicately scrubbing using a cotton swab, while the cells located at the filter's lower section were dyed for 60 min in a crystal violet solution (Sigma, USA) with a concentration of 0.5 % (w/v). The cells that had migrated were observed using an optical microscope (Olympus, Japan).

ROS assay: To evaluate the levels of intracellular ROS, the ROS probe DHE (5 μm) was used for staining, followed by three washes with PBS after 10 min. Fluorescent microscopy was used to capture the images.

Quantitative real-time polymerase chain reaction: The manufacturer's protocol was followed to isolate total RNA from cell samples using TRIzol in a quantitative real-time polymerase chain reaction. The 1st Strand cDNA Synthesis Kit was used to produce initial cDNA, followed by cDNA amplification using SYBR Premix Ex *Taq*II. The thermocycling process consisted of an initial denaturation at 95 °C for 3 min, followed by 40 cycles at 95 °C for a duration of 5 s, and subsequently at 60 °C for a duration of 30 s. ACTB mRNA levels were used as the internal control to normalize the levels of mRNA. Supporting Table 1 contains the primer sequences for RT-qPCR. Relative levels of transcripts were normalized by the $2-\Delta\Delta Cq$ method.

Western Blotting: Cells were lysed using a lysis buffer (Byotime, China) that contained 1 % protease inhibitors (Byotime, China). SDS–PAGE was used to apply proteins, which were then electroblotted onto a membrane made of polyvinylidene difluoride. Next, the polyvinylidene difluoride membranes were obstructed using 5 % milk without fat and left to incubate overnight at a temperature of 4 °C with particular antibodies for ACTB, NEDD8, IκBα/p-IκBα, VEGF-A, Cyclin D1, and Cyclin D3 (1:1000, Cell Signaling, USA). Following incubation and rinsing, the membranes were treated with a goat anti-rabbit IgG antibody conjugated with horseradish peroxidase (1 1000, Cell Signaling, USA) for 1 h at a temperature of 23 °C. Detection of chemiluminescence was carried out utilizing a Western Blotting Detection kit for ECL (Tanon, China). The manufacturer's instructions were followed to visualize the proteins.

Generation of Diabetic Mice Wound Model: Approval for all animal studies was granted by the Institutional Animal Care and Use Committee (IACUC) of Tongji Medical College, Huazhong University of Science and Technology, for the generation of a wound model in mice with diabetes. To induce diabetes in male C57BL/6J mice (6 weeks old), a high-fat diet was given for 6 weeks, followed by daily intraperitoneal injections of streptozotocin (STZ; 40 mg kg^{-1} day^{-1}) for 7 days. Mice with a fasting blood glucose level exceeding 15.9 mmol/L in two consecutive measurements were classified as diabetic and utilized for subsequent experiments. In addition, the control group of normal mice received daily intraperitoneal injections of PBS for seven consecutive days. Sodium pentobarbital (50 mg/kg; Sigma Aldrich) was used to anesthetize the mice, and then full-thickness excised skin wounds measuring 1.0 × 1.0 cm were created on the mice's back. Multiple site subcutaneous injections received a total of 100 μL of drug or PBS around the wound. A transparent dressing (3 M, USA) was used to cover the wounds. Wounds were photographed using a digital camera on days 0, 3, 7, 10, and 14. ImageJ (Media Cybernetics, USA) was utilized to measure the extent of wound closure.

IHC Staining: 14 days after the operation, the wound tissue of mice was collected for paraffin embedding and CD31 staining. The antigens were fixed in citrate buffer for a duration of 15 min and subsequently obstructed using goat serum for a period of 30 min. The sections were subjected to treatment with an anti-CD31 antibody (1:100; Abcam, ab28364) overnight at 4 °C. Afterwards, they were stained and counterstained using DAB and hematoxylin. The number of $CD31^+$ cells was counted under a microscope to evaluate micro-vascularization at the wound sites.

Immunofluorescence: After 14 days, mouse wound tissues were embedded in paraffin and sectioned. Immunofluorescence staining was conducted to detect the expression levels of iNOS and Arg1 proteins (1:200, Abcam). The influence of the nanoparticle drug delivery system on the macrophage phenotype was evaluated.

Histological Analysis: Samples of wound tissue were obtained on days 3, 7, and 14 for histological analysis. The samples were then treated with 4 % paraformaldehyde, dehydrated, and embedded in paraffin sections. After removing the paraffin, the sections were subjected to staining using hematoxylin and eosin (H&E) as well as Masson's trichrome (MT) dye.

Small Animal Doppler: The small animal Doppler was used to evaluate the blood circulation of the wounds 10 days post-surgery. In short, mice were administered sodium pentobarbital for anesthesia. Doppler examination (ROI 1) was used to measure the average blood perfusion in the mice's wound region. Mean perfusion rates were calculated by comparing ROI-1 values with mean blood perfusion values in the surrounding skin.

Statistical analysis: The statistical analysis involved expressing the quantitative data as the mean ± standard deviation (SD) and conducting the analysis using SPSS 19.0.0 software. The data was examined using either a two-tailed student's t-test or a one-way ANOVA. The difference was considered significant at $P < 0.05$. A minimum of three repetitions were conducted for all experiments.

Approval of ethics and agreement to participate

This study adhered to the European Community guidelines. The Institutional Animal Care and Use Committee (IACUC) of Tongji Medical College, Huazhong University of Science and Technology approved all animal experiments.

Funding

This work was supported by the National Science Foundation of China (No. 82272491, No. 82072444); the Wuhan Science and Technology Bureau (2022020801020464); the Department of Science and Technology of Hubei Province (No. 2021CFB425); Chinese Pharmaceutical Association Hospital Pharmacy department (No. CPA-Z05-ZC-2022-002); Hubei Province Unveiling Science and Technology Projects (No. 2022-35); Natural Science Foundation of Shenzhen Municipality (JCYJ20220531094802005); Medical Research Foundation of Guangdong Province (B2022242); Scientific Research Project in Health System of Pingshan District (202218).

Ethics approval and consent to participate

The experimental protocol was established, according to the ethical guidelines of the Helsinki Declaration. All animal experiments were approved by the Institutional Animal Care and Use Committee (IACUC) of Tongji Medical College, Huazhong University of Science and Technology.

Conflicts of interest

The manuscript has not been published elsewhere and is not being considered for publication by any other journal. All authors have read and approved this paper, as well as contributed to its content. There are no conflicts of interest. I am willing to assign copyright to the publisher, if the article is accepted.

CRediT authorship contribution statement

Ruiyin Zeng: Writing – original draft, Visualization, Validation, Methodology, Conceptualization. **Bin Lv:** Methodology, Validation, Writing – review & editing. **Ze Lin:** Writing – original draft, Investigation, Formal analysis, Conceptualization. **Xiangyu Chu:** Writing – original draft, Investigation, Data curation, Conceptualization. **Yuan Xiong:** Writing – original draft, Methodology, Formal analysis, Conceptualization. **Samuel Knoedler:** Software, Investigation, Formal

analysis. **Faqi Cao:** Visualization, Supervision, Methodology. **Chuanlu Lin:** Validation, Methodology. **Lang Chen:** Validation, Software. **Chenyan Yu:** Visualization, Software. **Jiewen Liao:** Validation. **Wu Zhou:** Software, Methodology. **Guandong Dai:** Writing – review & editing, Supervision, Project administration, Formal analysis. **Mohammad-Ali Shahbazi:** Writing – review & editing, Supervision, Project administration, Formal analysis. **Bobin Mi:** Writing – review & editing, Supervision, Formal analysis, Conceptualization. **Guohui Liu:** Writing – review & editing, Supervision, Funding acquisition, Formal analysis, Conceptualization.

Acknowledgements

Scheme 1, Fig. 3A, Fig. 4A, Fig. 6A were created with BioRender.com. Dr. M. -A. S acknowledges Incentive and Starterbeurs funds from the University of Groningen and UMCG.

Appendix A. Supplementary data

Supplementary data to this article can be found online at https://doi.org/10.1016/j.bioactmat.2023.12.025.

References

[1] Shape the future of diabetes at the IDF world diabetes congress 2022, Diabetes Res. Clin. Pract. 187 (2022) 109909.
[2] M.G. Tinajero, V.S. Malik, An update on the epidemiology of type 2 diabetes: a global perspective, Endocrinol Metab. Clin. N. Am. 50 (3) (2021) 337–355.
[3] A. Ceriello, Hyperglycaemia and the vessel wall: the pathophysiological aspects on the atherosclerotic burden in patients with diabetes, Eur. J. Cardiovasc. Prev. Rehabil. 17 (Suppl 1) (2010) S15–S19.
[4] D.F. Bandyk, The diabetic foot: pathophysiology, evaluation, and treatment, Semin. Vasc. Surg. 31 (2–4) (2018) 43–48.
[5] E. Manchon, N. Hirt, J.D. Bouaziz, N. Jabrane-Ferrat, R. Al-Daccak, Stem cells-derived extracellular vesicles: potential therapeutics for wound healing in chronic inflammatory skin diseases, Int. J. Mol. Sci. 22 (6) (2021).
[6] A.E. Louiselle, S.M. Niemiec, C. Zgheib, K.W. Liechty, Macrophage polarization and diabetic wound healing, Transl. Res. 236 (2021) 109–116.
[7] W.R. Francis, Z. Liu, S.E. Owens, X. Wang, H. Xue, A. Lord, et al., Role of hypoxia inducible factor 1α in cobalt nanoparticle induced cytotoxicity of human THP-1 macrophages, Biomater Transl. 2 (2) (2021) 143–150.
[8] R.I. Enchev, B.A. Schulman, M. Peter, Protein neddylation: beyond cullin-RING ligases, Nat. Rev. Mol. Cell Biol. 16 (1) (2015) 30–44.
[9] J. Zhu, F. Chu, M. Zhang, W. Sun, F. Zhou, Association between neddylation and immune response, Front. Cell Dev. Biol. 10 (2022) 890121.
[10] T.A. Soucy, P.G. Smith, M.A. Milhollen, A.J. Berger, J.M. Gavin, S. Adhikari, et al., An inhibitor of NEDD8-activating enzyme as a new approach to treat cancer, Nature 458 (7239) (2009) 732–736.
[11] Y.C. Zheng, Y.J. Guo, B. Wang, C. Wang, M.A.A. Mamun, Y. Gao, et al., Targeting neddylation E2s: a novel therapeutic strategy in cancer, J. Hematol. Oncol. 14 (1) (2021) 57.
[12] W. Hua, C. Li, Z. Yang, L. Li, Y. Jiang, G. Yu, et al., Suppression of glioblastoma by targeting the overactivated protein neddylation pathway, Neuro Oncol. 17 (10) (2015) 1333–1343.
[13] Z. Luo, G. Yu, H.W. Lee, L. Li, L. Wang, D. Yang, et al., The Nedd8-activating enzyme inhibitor MLN4924 induces autophagy and apoptosis to suppress liver cancer cell growth, Cancer Res. 72 (13) (2012) 3360–3371.
[14] X. Zhou, M. Tan, M.K. Nyati, Y. Zhao, G. Wang, Y. Sun, Blockage of neddylation modification stimulates tumor sphere formation in vitro and stem cell differentiation and wound healing in vivo, Proc. Natl. Acad. Sci. U. S. A. 113 (21) (2016) E2935–E2944.
[15] F.M. Chang, S.M. Reyna, J.C. Granados, S.J. Wei, W. Innis-Whitehouse, S.K. Maffi, et al., Inhibition of neddylation represses lipopolysaccharide-induced proinflammatory cytokine production in macrophage cells, J. Biol. Chem. 287 (42) (2012) 35756–35767.
[16] L. Li, B. Liu, T. Dong, H.W. Lee, J. Yu, Y. Zheng, et al., Neddylation pathway regulates the proliferation and survival of macrophages, Biochem. Biophys. Res. Commun. 432 (3) (2013) 494–498.
[17] M.A. Mofazzal Jahromi, P. Sahandi Zangabad, S.M. Moosavi Basri, K. Sahandi Zangabad, A. Ghamarypour, A.R. Aref, et al., Nanomedicine and advanced technologies for burns: preventing infection and facilitating wound healing, Adv. Drug Deliv. Rev. 123 (2018) 33–64.
[18] D. Dixon, M. Edmonds, Managing diabetic foot ulcers: pharmacotherapy for wound healing, Drugs 81 (1) (2021) 29–56.
[19] P. Wu, Y. Liang, G. Sun, Engineering immune-responsive biomaterials for skin regeneration, Biomater Transl. 2 (1) (2021) 61–71.
[20] R.K. Thapa, D.B. Diep, H.H. Tønnesen, Topical antimicrobial peptide formulations for wound healing: current developments and future prospects, Acta Biomater. 103 (2020) 52–67.
[21] J. Wang, X. Li, S. Wang, J. Cui, X. Ren, J. Su, Bone-Targeted exosomes: strategies and applications, Adv. Healthcare Mater. 12 (18) (2023) e2203361.
[22] F. Chen, F. Pu, Implantable immune stents: a new opportunity for cancer treatment, Biomater Transl. 4 (1) (2023) 3–4.
[23] L. Chen, Y. Xiong, Y.Q. Hu, C.Y. Yu, A.C. Panayi, W. Zhou, et al., Regulatory T cell-exosomal miR-142-3p promotes angiogenesis and osteogenesis via TGFBR1/SMAD2 inhibition to accelerate fracture repair, Chem. Eng. J. (2022) 427.
[24] L. Hu, X. Xie, H. Xue, T. Wang, A.C. Panayi, Z. Lin, et al., MiR-1224-5p modulates osteogenesis by coordinating osteoblast/osteoclast differentiation via the Rap1 signaling target ADCY2, Exp. Mol. Med. 54 (7) (2022) 961–972.
[25] Y. Xiong, L. Chen, P. Liu, T. Yu, C. Lin, C. Yan, et al., All-in-One: multifunctional hydrogel accelerates oxidative diabetic wound healing through timed-release of exosome and fibroblast growth factor, Small 18 (1) (2022) e2104229.
[26] R.H. Fang, Y. Jiang, J.C. Fang, L. Zhang, Cell membrane-derived nanomaterials for biomedical applications, Biomaterials 128 (2017) 69–83.
[27] X. Ren, X. Chen, Z. Geng, J. Su, Bone-targeted biomaterials: strategies and applications, Chem. Eng. J. 446 (2022) 137133.
[28] S. Wang, D. Wang, Y. Duan, Z. Zhou, W. Gao, L. Zhang, Cellular nanosponges for biological neutralization, Adv. Mater. 34 (13) (2022) e2107719.
[29] C. Yin, Q. Zhao, W. Li, Z. Zhao, J. Wang, T. Deng, et al., Biomimetic anti-inflammatory nano-capsule serves as a cytokine blocker and M2 polarization inducer for bone tissue repair, Acta Biomater. 102 (2020) 416–426.
[30] W. Chen, M. Schilperoort, Y. Cao, J. Shi, I. Tabas, W. Tao, Macrophage-targeted nanomedicine for the diagnosis and treatment of atherosclerosis, Nat. Rev. Cardiol. 19 (4) (2022) 228–249.
[31] S. Thamphiwatana, P. Angsantikul, T. Escajadillo, Q. Zhang, J. Olson, B.T. Luk, et al., Macrophage-like nanoparticles concurrently absorbing endotoxins and proinflammatory cytokines for sepsis management, Proc. Natl. Acad. Sci. U. S. A. 114 (43) (2017) 11488–11493.
[32] W.B. Horton, E.J. Barrett, Microvascular dysfunction in diabetes mellitus and cardiometabolic disease, Endocr. Rev. 42 (1) (2021) 29–55.
[33] N. Sawada, Z. Arany, Metabolic regulation of angiogenesis in diabetes and aging, Physiology 32 (4) (2017) 290–307.
[34] C. Chen, L. Gu, D.J. Matye, Y.D. Clayton, M.N. Hasan, Y. Wang, et al., Cullin neddylation inhibitor attenuates hyperglycemia by enhancing hepatic insulin signaling through insulin receptor substrate stabilization, Proc. Natl. Acad. Sci. U. S. A. 119 (6) (2022).
[35] Y. Zhang, Q. Guo, G. Jiang, C. Zhang, Dysfunction of Cullin 3 RING E3 ubiquitin ligase causes vasoconstriction and increased sodium reabsorption in diabetes, Arch. Biochem. Biophys. 710 (2021) 109000.
[36] A.C. Andérica-Romero, J. Hernández-Damián, G.I. Vázquez-Cervantes, I. Torres, I. G. González-Herrera, J. Pedraza-Chaverri, The MLN4924 inhibitor exerts a neuroprotective effect against oxidative stress injury via Nrf2 protein accumulation, Redox Biol. 8 (2016) 341–347.
[37] L. Cañedo-Dorantes, M. Cañedo-Ayala, Skin acute wound healing: a comprehensive review, Int. J. Inflamm. 2019 (2019) 3706315.
[38] L.M. Morton, T.J. Phillips, Wound healing and treating wounds: differential diagnosis and evaluation of chronic wounds, J. Am. Acad. Dermatol. 74 (4) (2016) 589–605, quiz -6.
[39] A.G. Kurian, R.K. Singh, K.D. Patel, J.H. Lee, H.W. Kim, Multifunctional GelMA platforms with nanomaterials for advanced tissue therapeutics, Bioact. Mater. 8 (2022) 267–295.
[40] B.J. Klotz, D. Gawlitta, A. Rosenberg, J. Malda, F.P.W. Melchels, Gelatin-methacryloyl hydrogels: towards biofabrication-based tissue repair, Trends Biotechnol. 34 (5) (2016) 394–407.
[41] S. Yi, Q. Liu, Z. Luo, J.J. He, H.L. Ma, W. Li, et al., Micropore-forming gelatin methacryloyl (GelMA) bioink toolbox 2.0: designable tunability and adaptability for 3D bioprinting applications, Small 18 (25) (2022) e2106357.
[42] M. Cano Sanchez, S. Lancel, E. Boulanger, R. Neviere, Targeting oxidative stress and mitochondrial dysfunction in the treatment of impaired wound healing: a systematic review, Antioxidants 7 (8) (2018).
[43] H. Xiu, Y. Peng, X. Huang, J. Gong, J. Yang, J. Cai, et al., Neddylation alleviates methicillin-resistant Staphylococcus aureus infection by inducing macrophage reactive oxygen species production, J. Immunol. 207 (1) (2021) 296–307.
[44] Y. Liang, Y. Jiang, X. Jin, P. Chen, Y. Heng, L. Cai, et al., Neddylation inhibition activates the protective autophagy through NF-κB-catalase-ATF3 Axis in human esophageal cancer cells, Cell Commun. Signal. 18 (1) (2020) 72.
[45] C. Schwechheimer, NEDD8-its role in the regulation of Cullin-RING ligases, Curr. Opin. Plant Biol. 45 (Pt A) (2018) 112–119.